Evolution of shape and collectivity along the Ge isotopic chain: The case of ^{80}Ge

D. Rhodes,[1,2,*] B. A. Brown,[1,2] A. Gade,[1,2] S. Biswas,[1,†] A. Chester,[1] P. Farris,[1,2] J. Henderson,[3] A. Hill ®,[1,2] J. Li,[1]
F. Nowacki,[4,5] E. Rubino ®,[1] D. Weisshaar ®,[1] and C. Y. Wu[6]

[1]*National Superconducting Cyclotron Laboratory, Michigan State University, East Lansing, Michigan 48824, USA*
[2]*Department of Physics and Astronomy, Michigan State University, East Lansing, Michigan 48824, USA*
[3]*Department of Physics, University of Surrey, Guildford, Surrey GU2 7XH, United Kingdom*
[4]*Université de Strasbourg, IPHC, 23 rue du Loess 67037 Strasbourg, France*
[5]*CNRS, UMR7178, 67200 Strasbourg, France*
[6]*Lawrence Livermore National Laboratory, Livermore, California 94550, USA*

The shape and collectivity of ^{80}Ge were investigated via a sub-barrier-energy Coulomb excitation measurement using the JANUS setup at the NSCL ReA3 facility. The ^{80}Ge spectroscopic quadrupole moment $Q_s(2_1^+)$ of the 2_1^+ state was measured for the first time, and the precision of the ^{80}Ge $B(E2; 0_1^+ \to 2_1^+)$ transition strength was increased. The experimental $Q_s(2_1^+)$ value indicates a large, prolate deformation for ^{80}Ge, which is consistent with large-scale shell-model calculations performed for comparison. These results provide important benchmarks for models that try to describe nuclear shape in neutron-rich nuclei near the magic number $N = 50$.

I. INTRODUCTION

The stable to neutron-rich isotopes of germanium are a critical testing ground for nuclear models due to their complex and rapidly changing nuclear structure. Near stability, the even-A $^{74-78}$Ge isotopes display triaxiality [1–5], while both shape coexistence [6] and triaxiality have been suggested for ^{72}Ge [7,8]. A transition from prolate to oblate deformation occurs at ^{70}Ge [9], and an additional region of triaxiality has been proposed around the neutron-rich ^{84,86,88}Ge isotopes [10]. Further, nuclei near the $N = 50$ isotone line, such as the very neutron-rich doubly magic nucleus ^{78}Ni [11], which is predicted to be at the entrance of a new island of inversion [12], have recently come into reach for *ab initio* type models [13]. This makes experimentally determined indicators of nuclear structure crucial as these models attempt to reach the even more neutron-rich nuclei which will become available at new-generation facilities such as the Facility for Rare Isotope Beams [14].

Two neutrons removed from $N = 50$, ^{80}Ge is important for a systematic understanding of neutron-rich nuclei in this region. Recent beyond-mean-field calculations [15], which compare well to the available data in the lighter Ge nuclei, have predicted a spherical configuration for magic $N = 50$ ^{82}Ge and a rapid onset of prolate deformation at both ^{80}Ge and ^{84}Ge. Sensitive measures of nuclear shape and deformation, such as $B(E2; 0_1^+ \to 2_1^+)$ transition strengths and $Q_s(2_1^+)$ quadrupole moments, are required to test these predictions and gain a detailed understanding of nuclear structure in

this important region of the nuclear chart. While the ^{80}Ge $B(E2; 0_1^+ \to 2_1^+)$ value is known [16,17], its quadrupole moment has not been measured to date.

The rare isotope ^{80}Ge has been studied with several different experimental techniques. Most recently, this nucleus attracted attention due to the reported observation of a surprisingly low-lying 0_2^+ state, in fact located below the 2_1^+ level [18]. This was subsequently refuted by another measurement searching for the conversion electron emitted by the reported 0_2^+ state's $E0$ decay [19]. A recent β-decay experiment [20] also found no evidence of the proposed low-lying 0_2^+ state.

Detailed information of the ^{80}Ge level scheme comes from β-decay [20,21] studies, while the isomeric 8_1^+ state was identified in a deep inelastic scattering measurement [22]. The lifetime of the 8_1^+ state was measured using fast-timing techniques [23]. Two Coulomb excitation experiments [16,17] measured the ^{80}Ge $B(E2; 0_1^+ \to 2_1^+)$, with Ref. [17] also measuring the $B(E2; 0_1^+ \to 2_2^+)$. These experiments were insensitive to the quadrupole moment, however, and accounting for the feeding from higher lying states was an additional complication in Ref. [17].

To test recent theoretical predictions [15] and track the evolution of nuclear shape toward $N = 50$, a sub-barrier-energy projectile Coulomb excitation experiment was performed to measure the ^{80}Ge $B(E2; 0_1^+ \to 2_1^+)$ transition strength and, for the first time, its spectroscopic quadrupole moment $Q_s(2_1^+)$. These values provide crucial benchmarks on nuclear shape and collectivity in neutron-rich nuclei near $N = 50$.

II. EXPERIMENTAL DETAILS AND DATA ANALYSIS

The present experiment was performed at the Reaccelerator facility (ReA3) [24] of the National Superconducting Cyclotron Laboratory (NSCL) [25]. An ^{82}Se primary

---

*Present address: TRIUMF, 4004 Wesbrook Mall, Vancouver, BC V6T 2A3, Canada; rhodesd@nscl.msu.edu

†Present address: Paul Scherrer Institute, Forschungsstrasse 111, 5232 Villigen, Switzerland.

beam was accelerated by the NSCL's coupled cyclotrons and impinged on a thick ^{9}Be production target to produce the cocktail secondary beam. The ^{80}Ge nuclei were selected using the A1900 fragment separator [26] and delivered to a gas cell [27], which is used to stop and thermalize the high-energy beam. The ^{80}Ge nuclei were extracted from the gas cell, charge bred in NSCL's electron-beam ion trap [28], and injected into the ReA3 accelerator to be delivered to the experimental setup.

The ^{80}Ge nuclei were impinged at 3.52 MeV/u on a 1.59 mg/cm^2 thick ^{196}Pt target. This is 98% of the "safe" energy restriction [29]. The use of a ^{196}Pt target provided target excitations which, along with its well-known spectroscopic data, were used to define the normalization necessary to measure matrix elements in ^{80}Ge. As ^{196}Pt is a high-Z nucleus, this method provided sensitivity to both the $Q_s(2_1^+)$ and $B(E2; 0_1^+ \rightarrow 2_1^+)$ values in ^{80}Ge.

The target position was surrounded by the Joint Array for Nuclear Structure (JANUS) [30], which combines two annular silicon detectors (Bambino2) with the Segmented Germanium Array (SeGA) [31]. The silicon detectors were placed 28(1) mm downstream and 32(1) mm upstream of the reaction target. They have 32-fold azimuthal segmentation on the side facing the target and 24-fold radial segmentation on the other. This geometry covers laboratory frame scattering angles of 21.4–51.3° (downstream) and 132–161° (upstream) with ≈1° localization in θ and 11.3° in ϕ. The silicon detectors were used to detect the scattered ^{80}Ge and the recoiling ^{196}Pt nuclei.

Sixteen 32-fold segmented detectors of SeGA were arranged in a compact "barrel" configuration, with the cylindrical detector crystals concentrically surrounding the target position. These were used to detect the prompt γ-ray decays from excited states of both nuclei and provided an absolute efficiency of 6.3% at 1 MeV.

At the time of the experiment, it was discovered that the ^{80}Ge beam contained about 7% contamination of stable ^{80}Kr, though the amount of contamination was observed to increase over the course of the experiment. This contamination was suspected to originate from the gas cell, and the contaminant ^{80}Kr nuclei were accelerated to the same energy as the ^{80}Ge. Since the energies and masses of both nuclei were the same, it was not possible to discriminate between the two beam species using the reaction kinematics measured by the silicon detectors.

The contaminant ^{80}Kr nuclei Coulomb excited the ^{196}Pt target, and the additional yield of ^{196}Pt γ rays would incorrectly change the normalization used for the ^{80}Ge excitations unless this contribution is removed. Because of this, a dedicated measurement was performed in which isotopically enriched ^{80}Kr gas was bled into the gas cell, producing a pure ^{80}Kr beam that was impinged on the ^{196}Pt target under identical experimental settings. This provided a direct measure of the ^{196}Pt γ-ray yields produced by the impinging ^{80}Kr contaminant.

The energy deposited in the forward silicon detector during the experiment is shown in Fig. 1. As is clearly seen, the kinematic curves of the scattered projectiles and the ^{196}Pt target recoils are well separated, which enables event-by-event characterization of the scattering process. It also clear from
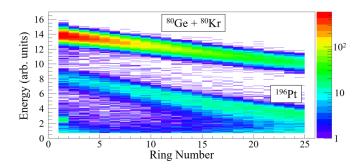

FIG. 1. The energy deposited in the downstream silicon detector. The scattered projectiles and recoiling ^{196}Pt nuclei are clearly visible and distinguishable. It is also clear there is no separation between the ^{80}Ge nuclei and the ^{80}Kr contamination.

Fig. 1 that the ^{80}Ge nuclei cannot be discriminated from the ^{80}Kr contamination using the measured reaction kinematics.

To increase the sensitivity of the measurement to the ^{80}Ge $Q(2_1^+)$ via the reorientation effect [29], the data were further subdivided into ranges based on the scattering angle. The γ-ray yields in coincidence with forward scattered ^{80}Ge were divided into three angular ranges, the data corresponding to ^{196}Pt detection were divided into two ranges, and the back-scattered ^{80}Ge data were considered as a whole. The choice of angular ranges was primarily motivated by the γ-ray statistics collected.

Doppler correction of the γ-ray data is enabled by the segmentation of SeGA and the silicon detectors as well as the known reaction kinematics. The velocity of the γ-ray emitter was calculated on an event-by-event basis by using the scattering angle measured with the silicon detectors; for both the scattered beam and recoiling target nuclei, the range of velocities observed in this experiment was $0.03 \lesssim v/c \lesssim 0.08$. The total Doppler-corrected γ-ray spectra collected during the experiment are shown in Fig. 2.

Both the ^{80}Ge and ^{80}Kr $2_1^+ \rightarrow 0_1^+$ γ-ray transitions can be clearly identified in Fig. 2. Due to the dedicated ^{80}Kr measurement, the number of ^{196}Pt γ rays caused by the impinging ^{80}Kr can be determined directly from the number of ^{80}Kr $2_1^+ \rightarrow 0_1^+$ γ rays observed during the ^{80}Ge setting. This enabled the ^{80}Kr contribution to be removed in a subtraction process similar to Ref. [32]. Figure 2 also shows the results of the subtraction, which removes the additional γ-ray yield due to the impinging ^{80}Kr. The subtraction process results in larger transition matrix elements extracted for ^{80}Ge, as there are more ^{80}Ge excitations relative to the amount of ^{196}Pt excitations after the subtraction has been applied. The level scheme of ^{80}Ge relevant to this experiment is shown in Fig. 3.

The γ-ray yield data were analyzed via a joint use of the GOSIA and GOSIA2 codes [33,34]. The GOSIA2 code, which was developed specifically for a simultaneous analysis of projectile and target excitations, uses the spectroscopic data of ^{196}Pt along with its measured γ-ray yields to determine the normalization necessary for the ^{80}Ge excitations. The literature data used for ^{196}Pt is given in Table I. During the GOSIA2 analysis, the ^{80}Ge $\langle 0_1^+ \| E2 \| 2_1^+ \rangle$ and $\langle 2_1^+ \| E2 \| 2_1^+ \rangle$ matrix elements were manually scanned, while all other matrix elements in ^{80}Ge were fixed, and the GOSIA2 code was used to check
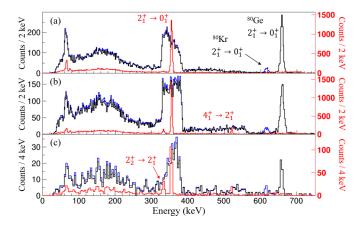
FIG. 2. Total γ-ray spectra collected during the experiment. The black and blue spectra are both Doppler corrected for ^{80}Ge; the γ rays from the ^{80}Kr contamination have been subtracted from the black spectra (see text), while the blue spectra have not been subtracted. Note the ^{80}Kr γ-ray transition is only present in the unsubtracted spectra. The red spectra are Doppler corrected for ^{196}Pt and have been subtracted. The panels show γ rays in coincidence with forward-scattered ^{80}Ge (a), forward-scattered ^{196}Pt (b), and back-scattered ^{80}Ge (c).

FIG. 3. The level scheme of ^{80}Ge used in the GOSIA and GOSIA2 analyses. Only transitions observed during the experiment are indicated. Energies are in keV.

the agreement between the calculated and experimental γ-ray yields. This results in a two-dimensional χ^2 surface, with the best-fit matrix elements given at the minimum χ^2 value and their individual 1-σ uncertainties given by a $\chi^2 < \chi^2_{\min} + 1$ cut.

Matrix elements which couple to states beyond the 2^+_1 were determined with the traditional GOSIA code. GOSIA only considers the ^{80}Ge γ-ray yields, so the best-fit ^{80}Ge $\langle 0^+_1 \| E2 \| 2^+_1 \rangle$ matrix element plus its uncertainty, extracted from the GOSIA2 analysis, is used as a fit constraint in order to define the required normalization. Due to the low population of the higher lying states, only weak sensitivity to the other matrix elements was observed and the joint GOSIA-GOSIA2 analysis rapidly converged. The final χ^2 surface obtained from the GOSIA2 analysis, after convergence of all matrix elements, is shown in Fig. 4.

Figure 4 shows the correlation between the $\langle 0^+_1 \| E2 \| 2^+_1 \rangle$ and $\langle 2^+_1 \| E2 \| 2^+_1 \rangle$ matrix elements which is typical in the Coulomb excitation of even-even nuclei [34,36]. For $\langle 0^+_1 \| E2 \| 2^+_1 \rangle$, this correlation was the dominant source of
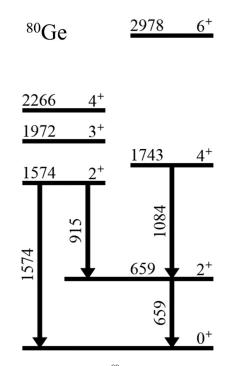
uncertainty beyond the simple statistical uncertainty from the γ-ray yields, which is also captured in the χ^2 surface. The $\langle 2^+_1 \| E2 \| 2^+_1 \rangle$ matrix element, however, displayed a significant correlation with matrix elements that couple to the 2^+_2 state; this effect is not observable in the χ^2 surface of Fig. 4. The matrix elements that couple to the 2^+_2 state had a negligible impact on the best-fit $\langle 0^+_1 \| E2 \| 2^+_1 \rangle$ value.

Figure 5 shows the effect of $\langle 2^+_1 \| E2 \| 2^+_2 \rangle$ on the best-fit $\langle 2^+_1 \| E2 \| 2^+_1 \rangle$, which determines the spectroscopic quadrupole moment $Q_s(2^+_1)$. This figure displays the total χ^2 value extracted from traditional GOSIA minimizations in which $\langle 2^+_1 \| E2 \| 2^+_2 \rangle$ and $\langle 2^+_1 \| E2 \| 2^+_1 \rangle$ were manually scanned, and the other relevant matrix elements in ^{80}Ge were allowed to vary. A standard $\chi^2 < \chi^2_{\min} + 1$ criterion reveals the weak sensitivity to $\langle 2^+_1 \| E2 \| 2^+_2 \rangle$ obtained from this experiment. The observed correlation results in a rather large and asymmetric uncertainty on the ^{80}Ge $\langle 2^+_1 \| E2 \| 2^+_1 \rangle$ [and thus on $Q_s(2^+_1)$]. This result highlights the possibly large effects of

TABLE I. The literature data [35] employed for ^{196}Pt during the GOSIA2 analysis. Uncertainties have been made symmetric for input into GOSIA2, and the diagonal matrix elements were derived from the quoted quadrupole moments.

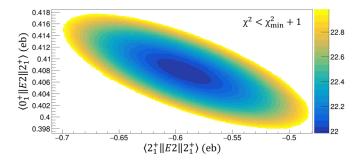| State	τ (ps)	Transitions	Branching ratio	Matrix element	Value (eb)	Transition	δ
2^+_1	49.27(22)	$4^+_2 \to 4^+_1 / 4^+_2 \to 2^+_2$	0.17(5)	$\langle 2^+_1 \| E2 \| 2^+_1 \rangle$	0.82(11)	$2^+_2 \to 2^+_1$	$-5.2(5)$
4^+_1	5.12(7)	$4^+_2 \to 2^+_1 / 4^+_2 \to 2^+_2$	0.17(2)	$\langle 4^+_1 \| E2 \| 4^+_1 \rangle$	1.37(16)		
6^+_1	1.41(12)	$0^+_2 \to 2^+_2 / 0^+_2 \to 2^+_1$	0.39(4)	$\langle 6^+_1 \| E2 \| 6^+_1 \rangle$	$-0.3(4)$		
8^+_1	0.61(6)	$3^+_1 \to 4^+_1 / 3^+_1 \to 2^+_2$	0.013(4)	$\langle 2^+_2 \| E2 \| 2^+_2 \rangle$	$-0.51(21)$		
0^+_2	6.1(14)	$3^+_1 \to 2^+_1 / 3^+_1 \to 2^+_2$	0.044(10)				
2^+_2	48.8(10)						
4^+_2	3.8(8)						
6^+_2	1.1(3)						

FIG. 4. The χ^2 surface, with a $\chi^2 < \chi^2_{min} + 1$ restriction, obtained from the GOSIA2 analysis which shows the correlation between the $\langle 0^+_1 \| E2 \| 2^+_1 \rangle$ and $\langle 2^+_1 \| E2 \| 2^+_1 \rangle$ matrix elements. All other matrix elements were fixed during this scan.

poorly-constrained matrix elements in multi-step Coulomb-excitation experiments, and it emphasizes the importance of investigating the possible correlations between matrix elements.

Beyond the correlation, Fig. 5 also reveals that there are two distinct solutions (local χ^2 minima) at $\langle 2^+_1 \| E2 \| 2^+_2 \rangle = \pm 0.52$ eb. Using the sign convention given in Fig. 5, these two solutions correspond to the two different signs of the P_3 triple product, which is given by

$$P_3 = \langle 0^+_1 \| E2 \| 2^+_1 \rangle \langle 2^+_1 \| E2 \| 2^+_2 \rangle \langle 2^+_2 \| E2 \| 0^+_1 \rangle. \quad (1)$$

The P_3 term is a common measure of quadrupole interference [37] which can significantly impact quadrupole moment determinations in multistep Coulomb excitation experiments depending on its sign [38,39]. As can been seen from Fig. 5, the present experiment indicates a preference for the $P_3 > 0$ solution, though it is not statistically significant at the 1-σ level. Thus, the relative signs of the matrix elements which form the P_3 triple product cannot be determined from this work, so the results suffer from this ambiguity.

It is interesting to note that, for either sign of P_3, the extracted ^{80}Ge $Q_s(2^+_1)$ value is negative. Several theoretical models, such as the triaxial rotor model with irrotational flow [40], the interacting boson model [41], and the anharmonic
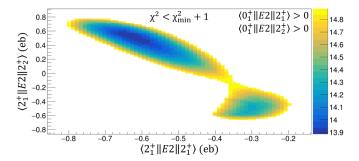

FIG. 5. The χ^2 surface, with a $\chi^2 < \chi^2_{min} + 1$ restriction, obtained from the traditional GOSIA code which shows the correlation between $\langle 2^+_1 \| E2 \| 2^+_1 \rangle$ and $\langle 2^+_1 \| E2 \| 2^+_2 \rangle$. At each point, GOSIA was used to minimize the other relevant matrix elements in ^{80}Ge. The observed correlation, combined with the presence of two distinct solutions (local χ^2 minima), results in large, highly asymmetric uncertainties on $\langle 2^+_1 \| E2 \| 2^+_1 \rangle$, i.e., $\langle 2^+_1 \| E2 \| 2^+_1 \rangle = -0.6^{+4}_{-2}$. The two solutions correspond to $\pm |P_3|$ (see text).
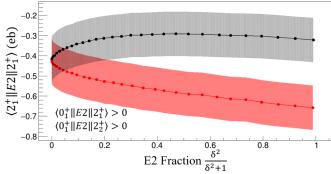

FIG. 6. The best-fit $\langle 2^+_1 \| E2 \| 2^+_1 \rangle$ value obtained for different assumptions of the $E2$ contribution to the mixed $E2/M1$ $2^+_2 \rightarrow 2^+_1$ γ-ray decay. The error bands, equal to ± 0.11 eb, give the uncertainty on $\langle 2^+_1 \| E2 \| 2^+_1 \rangle$ when ignoring correlations with matrix elements that couple to the 2^+_2 state. Using the given sign convention, the upper band (black) corresponds to $P_3 < 0$, and the lower band (red) corresponds to $P_3 > 0$.

vibrator model [39] all predict that the product $P_3 Q_s(2^+_1)$ is negative. The triaxial rotor model which does not assume irrotational flow can provide $P_3 Q_s(2^+_1) > 0$ [37,42]. Experimentally, many nuclei are known to display $P_3 Q_s(2^+_1) < 0$ (for example, Refs. [43,44]), including the even-A $^{70-76}$Ge isotopes [4,8,45,46]. Only the heavy, oblate ($Q_s(2^+_1) > 0$) nuclei ^{192,194}Pt are known unambiguously to exhibit $P_3 Q_s(2^+_1) > 0$; ^{74,76}Kr also display this property [47], though the presence of configuration mixing complicates the interpretation of these nuclei [37,47]. With this context, combined with the preference of the current measurement for $P_3 > 0$ (see Fig. 5), it is perhaps more likely that $P_3 > 0$ for ^{80}Ge.

In order to help constrain the matrix elements which couple to the 2^+_2 state, the adopted branching ratio of the 2^+_2 state's γ-ray transitions was incorporated into the GOSIA minimization. This value is $I_\gamma(2^+_2 \rightarrow 0^+_1)/I_\gamma(2^+_2 \rightarrow 2^+_1) = 0.83(5)$ [48]. To date, the multipole mixing ratio δ of the ^{80}Ge $2^+_2 \rightarrow 2^+_1$ γ-ray transition has not been measured. As such, the only sensitivity to $\langle 2^+_1 \| M1 \| 2^+_2 \rangle$ in this experiment is through the known branching ratio, which is also influenced by $\langle 2^+_1 \| E2 \| 2^+_2 \rangle$. Thus, the correlation presented in Fig. 5 can be expressed in terms of the $E2$ contribution to the mixed $E2/M1$ $2^+_2 \rightarrow 2^+_1$ γ-ray decay. The $E2$ fraction is given by $\delta^2/(\delta^2 + 1)$, and the correlation of $\langle 2^+_1 \| E2 \| 2^+_1 \rangle$ with this quantity is shown in Fig. 6. We stress that the current measurement provides no sensitivity to the relative sign of the $\langle 2^+_1 \| M1 \| 2^+_2 \rangle$ matrix element. Depending on the value, a measurement of δ would either strongly constrain the extracted $\langle 2^+_1 \| E2 \| 2^+_1 \rangle$ in ^{80}Ge, or it would provide two distinct solutions corresponding to $\pm |P_3|$. This can be seen from the two bands in Fig. 6 which converge for a small $E2$ contribution.

III. RESULTS AND DISCUSSION

All matrix elements extracted from this analysis are summarized in Table II, and the ^{80}Ge $B(E2; 0^+_1 \rightarrow 2^+_1)$ and $Q_s(2^+_1)$ values are shown in Table III. Comparison with previous measurements are provided where possible. While the

TABLE II. All matrix elements in ^{80}Ge determined from this work compared with previous measurements [16,17]. Absolute value symbols indicate that the relative sign of a matrix element could not be determined.

Matrix element	This work	Ref. [16]	Ref. [17]
$\langle 0_1^+ \| E2 \| 2_1^+ \rangle$ (eb)	0.408(10)	0.373(36)	0.316(21)
$\langle 2_1^+ \| E2 \| 2_1^+ \rangle$ (eb)	-0.6^{+4}_{-2}		
$\langle 2_1^+ \| E2 \| 4_1^+ \rangle$ (eb)	0.76(20)		
$\langle 0_1^+ \| E2 \| 2_2^+ \rangle$ (eb)	$\|0.14(5)\|$		$\|0.11(2)\|$
$\langle 2_1^+ \| E2 \| 2_2^+ \rangle$ (eb)	$<\|0.8\|$		
$\langle 2_1^+ \| M1 \| 2_2^+ \rangle$ (μ_{N})	$<\|0.5\|$		

current result for the $B(E2; 0_1^+ \to 2_1^+)$ transition strength is larger than the previous two measurements, it agrees with Ref. [16] within uncertainties, and the trend along the Ge isotope chain (see Fig. 8) displays a smooth decrease of $B(E2)$ with increasing N out to magic $N = 50$ ^{82}Ge. This agrees with conventional arguments from both a shell-model and a collective model point of view.

Multiple large-scale shell-model calculations were performed in order to further investigate the collectivity in ^{80}Ge. Two sets of calculations were performed with the NUSHELLX code [49]. Both sets of calculations employed the jj44 model space which consists of the $(0f_{7/2}, 1p_{3/2}, 1p_{1/2}, 0g_{9/2})$ orbitals for both protons and neutrons, and effective charges of $e_p = 1.8$ and $e_n = 0.8$ were used. These calculations used the jj44b and JUN45 [50] interactions, which have been widely employed to study germanium isotopes [51,52].

Additional shell-model calculations were performed using the LNPS [53] and PFSDG-U [12] interactions. The results of a calculation with a five-dimensional collective Hamiltonian (5DCH) with the Gogny D1S interaction [54] are presented as well. The comparison between the experimental and calculated results for the ^{80}Ge $B(E2; 0_1^+ \to 2_1^+)$ and $Q_s(2_1^+)$ values are also given in Table III.

As can be seen from Table III, the JUN45 and PFSDG-U calculations reproduce the current experimental values most closely. Both the jj44b and JUN45 interactions predict a quadrupole moment of -0.3 eb, but the jj44b interaction

TABLE III. Results for ^{80}Ge determined from this work compared with previous measurements [16,17] and to theoretical predictions.

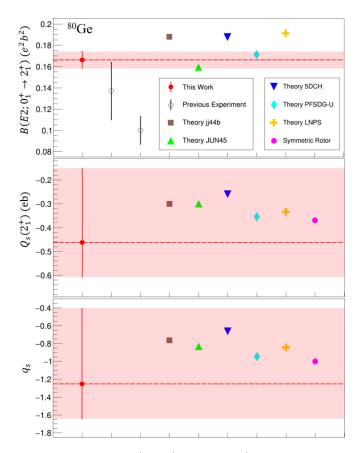| ^{80}Ge	$B(E2; 0_1^+ \to 2_1^+)$ (e^2b^2)	$Q_s(2_1^+)$ (eb)	q_s
Experiment			
This Work	0.166(8)	-0.46^{+31}_{-14}	-1.3^{+8}_{-4}
Ref. [16]	0.139(27)		
Ref. [17]	0.100(13)		
Theory			
jj44b	0.188	-0.301	-0.77
JUN45	0.159	-0.300	-0.83
PFSDG-U	0.171	-0.355	-0.95
LNPS	0.191	-0.334	-0.84
5DCH	0.188	-0.260	-0.66

FIG. 7. The $B(E2; 0_1^+ \to 2_1^+)$ (top), $Q_s(2_1^+)$ (middle), and q_s (bottom) values for ^{80}Ge from this work (red) compared to previous measurements and model predictions.

overpredicts the $B(E2; 0_1^+ \to 2_1^+)$ while the JUN45 interaction reproduces the transition strength quite well. The LNPS and PFSDG-U interactions predict slightly larger quadrupole moments; however, LNPS also overpredicts the $B(E2; 0_1^+ \to 2_1^+)$ value. The PFSDG-U interaction gives the best overall description of ^{80}Ge, though the large uncertainty on $Q_s(2_1^+)$ makes discriminating between the models difficult.

Irrespective of the large uncertainty, the present measurement indicates a larger $Q_s(2_1^+)$ value than all shell-model predictions. To explore this result, it is useful to consider the "reduced" quadrupole moment q_s, given by

$$q_s = \frac{Q_s(2_1^+)}{\frac{2}{7}\sqrt{\frac{16\pi}{5}} B(E2; 0_1^+ \to 2_1^+)}. \qquad (2)$$

The ratio q_s represents the size of the spectroscopic quadrupole moment $Q_s(2_1^+)$ relative to the prediction for an axially symmetric rigid rotor [40]. It is closely related to the quadrupole asymmetry parameter, which can be calculated from the quadrupole rotational invariants [29,55], and as such q_s is an indicator of axially symmetric or triaxial shapes. The value $q_s = 1$ indicates oblate axial symmetry, $q_s = -1$ indicates prolate axial symmetry, while all intermediate values $-1 < q_s < 1$ indicate triaxiality.

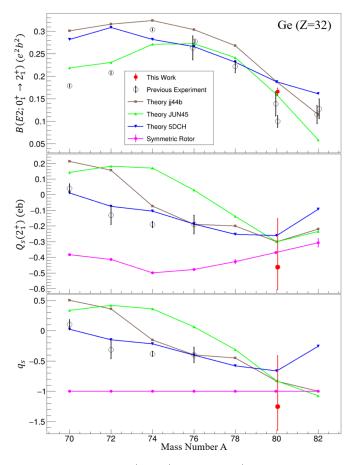Table III also gives the present result for the ^{80}Ge q_s compared to model predictions. The measured ^{80}Ge q_s is

FIG. 8. The $B(E2; 0_1^+ \to 2_1^+)$ (top), $Q_s(2_1^+)$ (middle), and q_s (bottom) values in the stable to neutron-rich germanium isotopes, with the present results in red. The experimental data are from Refs. [16,17,56,57]. The prolate symmetric rotor predictions and uncertainties for $Q_s(2_1^+)$ are based on the experimental $B(E2; 0_1^+ \to 2_1^+)$ values (the current result is used for ^{80}Ge).

larger than the axially symmetric rotor value, while all models predict some degree of triaxiality. The PFSDG-U calculation provides the largest magnitude of q_s and thus agrees best with the current result, though again the large uncertainty makes discriminating among the models difficult. Figure 7 shows the current result for the ^{80}Ge $B(E2; 0_1^+ \to 2_1^+)$, $Q_s(2_1^+)$, and q_s values compared to previous measurements and model predictions.

To see if the difference between experiment and theory for $Q_s(2_1^+)$ and q_s can be understood, the jj44b and JUN45 shell-model calculations were performed for the stable to neutron-rich even-A $^{70-82}$Ge isotopes. The results are shown in Fig. 8, which also includes the $Q_s(2_1^+)$ expected for an axially symmetric prolate rigid rotor from the experimentally determined $B(E2; 0_1^+ \to 2_1^+)$ values.

From the top panel of Fig. 8, the evolution of collectivity in the heavy Ge isotopes is well reproduced by the shell-model calculations, though the jj44b interaction consistently overpredicts the $B(E2; 0_1^+ \to 2_1^+)$ transition strengths until ^{82}Ge. The JUN45 calculations reproduce the $B(E2; 0_1^+ \to 2_1^+)$ values of $^{76-80}$Ge very well, though it underpredicts the collectivity of ^{82}Ge. The lighter Ge isotopes are not as well

described by the calculations, though JUN45 gives the best overall description of the isotopic chain.

The spectroscopic quadrupole moments, shown in the middle panel of Fig. 8, reveal larger discrepancies between experiment and theory. However, both shell-model calculations predict a local minimum at ^{80}Ge and a rapid increase of $Q_s(2_1^+)$ with decreasing mass number. This general behavior is consistent with the current result for ^{80}Ge as well as the data for the lighter Ge isotopes. Though the quadrupole moments prove challenging for both sets of shell-model calculations, the jj44b interaction describes the overall evolution of $Q_s(2_1^+)$ best.

As mentioned, not only is the experimental ^{80}Ge $Q_s(2_1^+)$ larger than the shell-model calculations, it is also larger than the prediction for a prolate rigid rotor (though the error bar overlaps with all theoretical values). As such, the current results for ^{80}Ge indicate a rapid onset of a very strong prolate deformation just two neutrons removed from magic $N = 50$. The lighter $^{72-76}$Ge isotopes have smaller quadrupole moments, despite having larger $B(E2; 0_1^+ \to 2_1^+)$ transition strengths, due to the triaxial nature of their deformation. The present experimental result is a first indication that ^{80}Ge does not exhibit significant triaxiality and instead points to rapid structural change in the heavy Ge isotopes. Measurement of the quadrupole moments in ^{78,82}Ge would be very beneficial to confirm and quantify this rapid evolution of shape.

IV. SUMMARY

In summary, a sub-barrier-energy Coulomb excitation experiment on ^{80}Ge was performed at the NSCL ReA3 facility using the JANUS setup. The ^{80}Ge $Q_s(2_1^+)$ and $B(E2; 0_1^+ \to 2_1^+)$ values were measured, and the results indicate a large prolate deformation of ^{80}Ge just two neutrons removed from magic $N = 50$. Shell-model calculations performed for comparison reproduce both current result for the ^{80}Ge $B(E2; 0_1^+ \to 2_1^+)$ transition strength as well as the trend in the heavy isotopes. The quadrupole moments proved more challenging for theory, though both sets of shell-model calculations performed for $^{70-82}$Ge point to a larger prolate deformation in ^{80}Ge compared to its neighboring isotopes. The present measurement is consistent with this picture.

[1] J. J. Sun, Z. Shi, X. Q. Li, H. Hua, C. Xu, Q. B. Chen, S. Q. Zhang, C. Y. Song, J. Meng, X. G. Wu, S. P. Hu, H. Q. Zhang, W. Y. Liang, F. R. Xu, Z. H. Li, G. S. Li, C. Y. He, Y. Zheng, Y. L. Ye, D. X. Jiang *et al.*, Phys. Lett. B **734**, 308 (2014).

[2] S. Mukhopadhyay, B. P. Crider, B. A. Brown, S. F. Ashley, A. Chakraborty, A. Kumar, M. T. McEllistrem, E. E. Peters, F. M. Prados-Estévez, and S. W. Yates, Phys. Rev. C **95**, 014327 (2017).

[3] Y. Toh, C. J. Chiara, E. A. McCutchan, W. B. Walters, R. V. F. Janssens, M. P. Carpenter, S. Zhu, R. Broda, B. Fornal, B. P. Kay, F. G. Kondev, W. Krolas, T. Lauritsen, C. J. Lister, T. Pawlat, D. Seweryniak, I. Stefanescu, N. J. Stone, J. Wrzesinski, K. Higashiyama, and N. Yoshinaga, Phys. Rev. C **87**, 041304(R) (2013).

[4] A. D. Ayangeakaa, R. V. F. Janssens, S. Zhu, D. Little, J. Henderson, C. Y. Wu, D. J. Hartley, M. Albers, K. Auranen, B. Bucher, M. P. Carpenter, P. Chowdhury, D. Cline, H. L. Crawford, P. Fallon, A. M. Forney, A. Gade, A. B. Hayes, F. G. Kondev, Krishichayan *et al.*, Phys. Rev. Lett. **123**, 102501 (2019).

[5] A. M. Forney, W. B. Walters, C. J. Chiara, R. V. F. Janssens, A. D. Ayangeakaa, J. Sethi, J. Harker, M. Alcorta, M. P. Carpenter, G. Gürdal, C. R. Hoffman, B. P. Kay, F. G. Kondev, T. Lauritsen, C. J. Lister, E. A. McCutchan, A. M. Rogers, D. Seweryniak, I. Stefanescu, and S. Zhu, Phys. Rev. Lett. **120**, 212501 (2018).

[6] K. Heyde and J. L. Wood, Rev. Mod. Phys. **83**, 1467 (2011).

[7] B. Kotliński, T. Czosnyka, D. Cline, J. Srebrny, C. Y. Wu, A. Bäcklin, L. Hasselgren, L. Westerberg, C. Baktash, and S. G. Steadman, Nucl. Phys. A **519**, 646 (1990).

[8] A. D. Ayangeakaa, R. V. F. Janssens, C. Y. Wu, J. M. Allmond, J. L. Wood, S. Zhu, M. Albers, S. Almaraz-Calderon, B. Bucher, M. P. Carpenter, C. J. Chiara, D. Cline, H. L. Crawford, H. M. David, J. Harker, A. B. Hayes, C. R. Hoffman, B. P. Kay, K. Kolos, A. Korichi *et al.*, Phys. Lett. B **754**, 254 (2016).

[9] R. Lecomte, M. Irshad, S. Landsberger, P. Paradis, and S. Monaro, Phys. Rev. C **22**, 1530 (1980).

[10] M. Lettmann, V. Werner, N. Pietralla, P. Doornenbal, A. Obertelli, T. R. Rodríguez, K. Sieja, G. Authelet, H. Baba, D. Calvet, F. Château, S. Chen, A. Corsi, A. Delbart, J.-M. Gheller, A. Giganon, A. Gillibert, V. Lapoux, T. Motobayashi, M. Niikura *et al.*, Phys. Rev. C **96**, 011301 (2017).

[11] R. Taniuchi, C. Santamaria, P. Doornenbal, A. Obertelli, K. Yoneda, G. Authelet, H. Baba, D. Calvet, F. Château, A. Corsi, A. Delbart, J.-M. Gheller, A. Gillibert, J. D. Holt, T. Isobe, V. Lapoux, M. Matsushita, J. Menéndez, S. Momiyama, T. Motobayashi *et al.*, Nature (London) **569**, 53 (2019).

[12] F. Nowacki, A. Poves, E. Caurier, and B. Bounthong, Phys. Rev. Lett. **117**, 272501 (2016).

[13] G. Hagen, G. R. Jansen, and T. Papenbrock, Phys. Rev. Lett. **117**, 172501 (2016).

[14] T. Glasmacher, B. Sherrill, W. Nazarewicz, A. Gade, P. Mantica, J. Wei, G. Bollen, and B. Bull, Nucl. Phys. News **27**, 28 (2017).

[15] K. Nomura, R. Rodríguez-Guzmán, and L. M. Robledo, Phys. Rev. C **95**, 064310 (2017).

[16] E. Padilla-Rodal, A. Galindo-Uribarri, C. Baktash, J. C. Batchelder, J. R. Beene, R. Bijker, B. A. Brown, O. Castaños, B. Fuentes, J. G. del Campo, P. A. Hausladen, Y. Larochelle, A. F. Lisetskiy, P. E. Mueller, D. C. Radford, D. W. Stracener, J. P. Urrego, R. L. Varner, and C.-H. Yu, Phys. Rev. Lett. **94**, 122501 (2005).

[17] H. Iwasaki, S. Michimasa, M. Niikura, M. Tamaki, N. Aoi, H. Sakurai, S. Shimoura, S. Takeuchi, S. Ota, M. Honma, T. K. Onishi, E. Takeshita, H. J. Ong, H. Baba, Z. Elekes, T. Fukuchi, Y. Ichikawa, M. Ishihara, N. Iwasa, S. Kanno, R. Kanungo, S. Kawai, T. Kubo, K. Kurita, T. Motobayashi, A. Saito, Y. Satou, H. Suzuki, M. K. Suzuki, Y. Togano, and Y. Yanagisawa, Phys. Rev. C **78**, 021304(R) (2008).

[18] A. Gottardo, D. Verney, C. Delafosse, F. Ibrahim, B. Roussière, C. Sotty, S. Roccia, C. Andreoiu, C. Costache, M.-C. Delattre, I. Deloncle, A. Etilé, S. Franchoo, C. Gaulard, J. Guillot, M. Lebois, M. MacCormick, N. Marginean, R. Marginean, I. Matea *et al.*, Phys. Rev. Lett. **116**, 182501 (2016).

[19] F. H. Garcia, C. Andreoiu, G. C. Ball, A. Bell, A. B. Garnsworthy, F. Nowacki, C. M. Petrache, A. Poves, K. Whitmore, F. A. Ali, N. Bernier, S. S. Bhattacharjee, M. Bowry, R. J. Coleman, I. Dillmann, I. Djianto, A. M. Forney, M. Gascoine, G. Hackman, K. G. Leach *et al.*, Phys. Rev. Lett. **125**, 172501 (2020).

[20] S. Sekal, L. M. Fraile, R. Lică, M. J. G. Borge, W. B. Walters, A. Aprahamian, C. Benchouk, C. Bernards, J. A. Briz, B. Bucher, C. J. Chiara, Z. Dlouhý, I. Gheorghe, D. G. Ghiţă, P. Hoff, J. Jolie, U. Köster, W. Kurcewicz, H. Mach, N. Mărginean *et al.*, Phys. Rev. C **104**, 024317 (2021).

[21] P. Hoff and B. Fogelberg, Nucl. Phys. A **368**, 210 (1981).

[22] A. Makishima, M. Asai, T. Ishii, I. Hossain, M. Ogawa, S. Ichikawa, and M. Ishii, Phys. Rev. C **59**, R2331 (1999).

[23] H. Mach, P. M. Walker, R. Julin, M. Leino, S. Juutinen, M. Stanoiu, Z. Podolyak, R. Wood, A. M. Bruce, T. Bäck, J. A. Cameron, B. Cederwall, J. Ekman, B. Fogelberg, P. T. Greenless, M. Hellström, P. Jones, W. Klamra, K. Lagergren, A.-P. Leppänen *et al.*, J. Phys. G: Nucl. Part. Phys. **31**, S1421 (2005).

[24] A. C. C. Villari, D. Alt, G. Bollen, D. B. Crisp, M. Ikegami, S. W. Krause, A. Lapierre, S. M. Lidia, D. J. Morrissey, S. Nash, R. J. Rencsok, R. Ringle, S. Schwarz, R. Shane, C. Sumithrarachchi, S. J. Williams, and Q. Zhao, in *Proceedings of the International Particle Accelerator Conference (IPAC'16), Busan, Korea* (JACoW, Geneva, Switzerland, 2016), pp. 1287–1290.

[25] A. Gade and B. M. Sherrill, Phys. Scr. **91**, 053003 (2016).

[26] D. J. Morrissey, B. M. Sherrill, M. Steiner, A. Stolz, and I. Wiedenhoever, Nucl. Instrum. Methods Phys. Res. B **204**, 90 (2003).

[27] C. S. Sumithrarachchi, D. J. Morrissey, S. Schwarz, K. Lund, G. Bollen, R. Ringle, G. Savard, and A. C. C. Villari, Nucl. Instrum. Methods Phys. Res. B **463**, 305 (2020).

[28] A. Lapierre, G. Bollen, D. Crisp, S. W. Krause, L. E. Linhardt, K. Lund, S. Nash, R. Rencsok, R. Ringle, S. Schwarz, M. Steiner, C. Sumithrarachchi, T. Summers, A. C. C. Villari, S. J. Williams, and Q. Zhao, Phys. Rev. Accel. Beams **21**, 053401 (2018).

[29] D. Cline, Annu. Rev. Nucl. Part. Sci. **36**, 683 (1986).

[30] E. Lunderberg, J. Belarge, P. C. Bender, B. Bucher, D. Cline, B. Elman, A. Gade, S. N. Liddick, B. Longfellow, C. Prokop, D. Weisshaar, and C. Y. Wu, Nucl. Instrum. Methods Phys. Res. A **885**, 30 (2018).

[31] W. F. Mueller, J. A. Church, T. Glasmacher, D. Gutknecht, G. Hackman, P. G. Hansen, Z. Hu, K. L. Miller, and P. Quirin, Nucl. Instrum. Methods Phys. Res. A **466**, 492 (2001).

[32] L. Morrison, K. Hadyńska-Klek, Z. Podolyák, L. Gaffney, L. Kaya, T. Berry, A. Boukhari, M. Brunet, R. Canavan, R. Catherall, S. Colosimo, J. Cubiss, H. De Witte, D. Doherty, C. Fransen, E. Giannopoulos, H. Grawe, H. Hess, T. Kröll, and M. Zielińska, J. Phys.: Conf. Ser. **1643**, 012146 (2020).

[33] T. Czosnyka, D. Cline, and C. Y. Wu, Bull. Am. Phys. Soc. **28**, 745 (1983).

[34] M. Zielińska, L. P. Gaffney, K. Wrzosek-Lipska, E. Clément, T. Grahn, N. Kesteloot, P. Napiorkowski, J. Pakarinen, P. Van Duppen, and N. Warr, Eur. Phys. J. A **52**, 99 (2016).

[35] H. Xiaolong, Nucl. Data Sheets **108**, 1093 (2007).

[36] S. A. Gillespie, J. Henderson, K. Abrahams, F. A. Ali, L. Atar, G. C. Ball, N. Bernier, S. S. Bhattcharjee, R. Caballero-Folch, M. Bowry, A. Chester, R. Coleman, T. Drake, E. Dunling, A. B. Garnsworthy, B. Greaves, G. F. Grinyer, G. Hackman, E. Kasanda, R. LaFleur *et al.*, Phys. Rev. C **104**, 044313 (2021).

[37] J. M. Allmond, J. L. Wood, and W. D. Kulp, Phys. Rev. C **80**, 021303(R) (2009).

[38] R. G. Stokstad, I. Hall, G. D. Symons, and J. de Boer, Nucl. Phys. A **92**, 319 (1967).

[39] T. Tamura, Phys. Lett. B **28**, 90 (1968).

[40] A. S. Davydov and G. F. Filippov, Nucl. Phys. **8**, 237 (1958).

[41] A. Arima, T. Ohtsuka, F. Iachello, and I. Talmi, Phys. Lett. B **66**, 205 (1977).

[42] J. L. Wood, A.-M. Oros-Peusquens, R. Zaballa, J. M. Allmond, and W. D. Kulp, Phys. Rev. C **70**, 024308 (2004).

[43] L. Hasselgren, C. Fahlander, F. Falk, L. O. Edvardson, J. E. Thun, B. S. Ghuman, and B. Skaali, Nucl. Phys. A **264**, 341 (1976).

[44] L. E. Svensson, C. Fahlander, L. Hasselgren, A. Bäcklin, L. Westerberg, D. Cline, T. Czosnyka, C. Y. Wu, R. M. Diamond, and H. Kluge, Nucl. Phys. A **584**, 547 (1995).

[45] M. Sugawara, Y. Toh, T. Czosnyka, M. Oshima, T. Hayakawa, H. Kusakari, Y. Hatsukawa, J. Katakura, N. Shinohara, M. Matsuda, T. Morikawa, A. Seki, and F. Sakata, Eur. Phys. J. A **16**, 409 (2003).

[46] Y. Toh, T. Czosnyka, M. Oshima, T. Hayakawa, H. Kusakari, M. Sugawara, Y. Hatsukawa, J. Katakura, N. Shinohara, and M. Matsuda, Eur. Phys. J. A **9**, 353 (2000).

[47] E. Clement, A. Gorgen, W. Korten, E. Bouchez, A. Chatillon, J. P. Delaroche, M. Girod, H. Goutte, A. Hurstel, Y. L. Coz, A. Obertelli, S. Peru, C. Theisen, J. N. Wilson, M. Zielinska, C. Andreoiu, F. Becker, P. A. Butler, J. M. Casandjian, W. N. Catford, T. Czosnyka, G. D. France, J. Gerl, R. D. Herzberg, J. Iwanicki, D. G. Jenkins, G. D. Jones, P. J. Napiorkowski, G. Sletten, and C. N. Timis, Phys. Rev. C **75**, 054313 (2007).

[48] B. Singh, Nucl. Data Sheets **105**, 223 (2005).

[49] B. A. Brown and W. D. M. Rae, Nucl. Data Sheets **120**, 115 (2014).

[50] M. Honma, T. Otsuka, T. Mizusaki, and M. Hjorth-Jensen, Phys. Rev. C **80**, 064323 (2009).

[51] S. J. Q. Robinson, L. Zamick, and Y. Y. Sharon, Phys. Rev. C **83**, 027302 (2011).

[52] J. G. Hirsch and P. C. Srivastava, J. Phys.: Conf. Ser. **387**, 012020 (2012).

[53] S. M. Lenzi, F. Nowacki, A. Poves, and K. Sieja, Phys. Rev. C **82**, 054301 (2010).

[54] G. F. Bertsch, M. Girod, S. Hilaire, J.-P. Delaroche, H. Goutte, and S. Péru, Phys. Rev. Lett. **99**, 032502 (2007).

[55] K. Kumar, Phys. Rev. Lett. **28**, 249 (1972).

[56] BNL evaluated nuclear structure data file (ENSDF), https://www.nndc.bnl.gov.

[57] A. Gade, T. Baugher, D. Bazin, B. A. Brown, C. M. Campbell, T. Glasmacher, G. F. Grinyer, M. Honma, S. McDaniel, R. Meharchand, T. Otsuka, A. Ratkiewicz, J. A. Tostevin, K. A. Walsh, and D. Weisshaar, Phys. Rev. C **81**, 064326 (2010).